APL Materials

RESEARCH ARTICLE | NOVEMBER 19 2024

Large perpendicular magnetic anisotropy at Fe/rock-salt-type Cr-oxide interface synthesized via oxygen-driven chemical layer exchange process

Yuki Iida; Qingyi Xiang ; Thomas Scheike ; Zhenchao Wen ; Jun Okabayashi ; Jun Uzuhashi ; Tadakatsu Ohkubo ; Kazuhiro Hono ; Hiroaki Sukegawa ; Seiji Mitani

APL Mater. 12, 111116 (2024)
https://doi.org/10.1063/5.0233103

Large perpendicular magnetic anisotropy at Fe/rock-salt-type Cr-oxide interface synthesized via oxygen-driven chemical layer exchange process

Cite as: APL Mater. 12, 111116 (2024); doi: 10.1063/5.0233103
Submitted: 12 August 2024 • Accepted: 27 October 2024 •
Published Online: 19 November 2024

Yuki Iida,[1,2] Qingyi Xiang,[2] Thomas Scheike,[2] Zhenchao Wen,[2] Jun Okabayashi,[3,a)] Jun Uzuhashi,[2] Tadakatsu Ohkubo,[2] Kazuhiro Hono,[2] Hiroaki Sukegawa,[2,a)] and Seiji Mitani[1,2]

AFFILIATIONS

[1] Graduate School of Pure and Applied Sciences, University of Tsukuba, Tsukuba 305-8577, Japan
[2] Research Center for Magnetic and Spintronic Materials, National Institute for Materials Science (NIMS), Tsukuba 305-0047, Japan
[3] Research Center for Spectrochemistry, The University of Tokyo, Bunkyo-ku, Tokyo 113-0033, Japan

[a)] **Authors to whom correspondence should be addressed:** jun@chem.s.u-tokyo.ac.jp and sukegawa.hiroaki@nims.go.jp

ABSTRACT

Perpendicular magnetic anisotropy (PMA) induced at the interface of the metallic magnetic layer/oxide layer plays a major role in scaling of state-of-the-art spin-transfer-torque magnetoresistive random access memory. The realization of PMA requires the development of mature interface manipulation techniques as well as materials constituting the interface. Herein, we report large PMA using stacks developed with an ultrathin (~0.7 nm) Fe/rock-salt CrO(001) interface via an oxygen-driven diffusion process. The stacks were prepared by sputter-deposition and post-annealing of the Cr buffer/ultrathin Fe/MgO structure. Significant oxidation of the Fe layer and Cr diffusion into the MgO layer occurred during the deposition. After post-annealing, the oxidized Fe layer was reduced to form an Fe/rock-salt-type Cr-monoxide structure due to chemical layer exchange. The lattice-matched Fe/CrO interface with a large interfacial PMA energy of 1.55 mJ/m^2 was confirmed after annealing at 500 °C. X-ray absorption spectroscopy measurements revealed that the post-annealing promoted the redox reaction from the Fe oxide to the metallic Fe and the formation of the CrO. The observed PMA indicates that the oxygen-driven diffusion process by annealing resulted in the well-controlled Fe/CrO interface. The demonstrated diffusion process provides a new chemical route to fabricate artificial, well-controlled PMA interfaces, even containing metastable materials, beyond the conventional sequential layer stacking for the development of spintronic devices.

I. INTRODUCTION

Magnetic properties of ultrathin (typically 1 nm or less) ferromagnetic metal (FM)/oxide interfaces have been intensively studied in the field of spintronics, especially with respect to magnetic tunnel junctions (MTJs) with perpendicular magnetic anisotropy (PMA) at the interface. The ultrathin Fe-based FM/oxide systems, for example, CoFeB/MgO[1–3] and Fe/MgO, realize substantial interfacial PMA,[4,5] which is required for ultra-high density magnetoresistive random access memory (MRAM) applications, in addition to a large tunnel magnetoresistance (TMR) ratio[6–9] and a low-power magnetization switching by spin-transfer torque.[2,3,10] In particular, much effort has been devoted to the formation of polycrystalline perpendicularly magnetized MTJs (p-MTJs) using a CoFeB/MgO interface because of its practical advantage of being obtained on various types of underlayers and its good PMA properties.[1–3,11–15] A single-crystalline Fe/MgO(001) interface is also a promising structure for obtaining large interfacial PMA for p-MTJs. The interfacial PMA energy density K_i of ~2 mJ/m^2 has been demonstrated at the interface,[4,16] which exceeds the values at the CoFeB/MgO interface

(1.6–1.8 mJ/m^2).[17,18] At these interfaces, the chemical bonding plays an essential role for PMA through the interfacial symmetry breaking.[19–23] First-principles calculations indicate that the interfacial hybridization between Fe-3$d_z{}^2$ and O-2p_z states is the main origin of the large interfacial PMA.[21]

In addition to MgO, the search for suitable oxide layers to obtain large interfacial PMA with the FM layer could expand the variety of spintronic heterostructures for future applications; for example, a lattice-matched Fe/$MgAl_2O_4$(001) interface was reported to show a large K_i of ~1.7 mJ/m^2 (experiment)[24] and ~1.2 mJ/m^2 (theoretical calculation).[25] A $Co_2FeAl/MgAl_2O_4$ interface also showed a large K_i of 1.6 mJ/m^2. Interestingly, significant interfacial Al diffusion was observed at the $Co_2FeAl/MgAl_2O_4$ interface, and this modification enhanced the PMA due to the promoted interfacial hybridization of Fe and O orbitals.[26,27] Therefore, the atomic scale control of the FM/oxide interfaces is critical for improving the interfacial PMA properties. Recently, an Fe/NiO(001) interface shows PMA with K_i of 0.93 mJ/m^2.[28] Therefore, even 3*d*-transition metal-oxides could be a promising material family for achieving large interfacial PMA. Thus, the realization of PMA requires developing both mature interface manipulation techniques and materials constituting the interface.

In this study, we demonstrate the formation of an epitaxial ultrathin (~0.7 nm) Fe(001)/metastable rock-salt-type CrO(001)/MgO(001) structure using sputter deposition and post-annealing of an initially designed Cr-buffered/Fe/MgO multilayer. The nanostructural, magnetic, and chemical evolution with post-annealing temperature were carefully monitored. We employed the Cr buffer layer because it is widely used to obtain a flat surface of an ultrathin Fe(001) layer due to its small lattice mismatch with Fe.[4,9,24] However, we found that the oxygen-induced diffusion process occurs during the post-annealing, resulting in chemical layer exchange and redox reaction within the stack. This process eventually led to the formation of a chemically sharp Fe/CrO(001) interface with a relatively small lattice mismatch. The formed Fe/CrO interface exhibited a large K_i of 1.55 mJ/m^2 after post-annealing at 500 °C, indicating that CrO is a promising oxide for PMA heterostructures. Our findings on the formation of a sharp interface with a 3*d* transition metal-oxide layer provide a way to fabricate stable PMA interfaces toward the development of spintronic devices.

II. EXPERIMENTS

The sputtered samples with a structure of MgO buffer (5 nm)/Cr buffer (30 nm)/Fe (0.7 nm)/MgO barrier (2 nm)/Ru cap were deposited on a MgO(001) substrate by ultra-high vacuum rf magnetron sputtering (base pressure: ~10^{-6} Pa). The sputtering pressure of Ar gas (99.999%), the sputtering power for 76.2 mm diameter targets, and the deposition rate are as follows: 0.5 Pa, 50 W, 0.025 nm/s for Fe, 0.5 Pa, 50 W, 0.033 nm/s for Cr, and 0.5 Pa, 100 W, 0.013 nm/s for MgO. The substrate–target distance was fixed at 100 mm. The substrate temperature during the sputter-deposition for each layer was room temperature. Prior to deposition, the MgO substrate was pre-heated to 500 °C for surface cleaning. After the Cr buffer deposition, the samples were annealed *in situ* at 500 °C to obtain a flat surface and (001) orientation. Some of the samples were post-annealed *ex-situ* at the annealing temperature (T_a) of 300, 400, or 500 °C for 1 h in the sputtering chamber. We also prepared electron-beam (EB)-grown samples (EB sample) with the same stack structure for comparison. For the EB sample, the MgO substrates and Cr buffer were annealed *in situ* at 800 °C, and the Fe and MgO barrier were annealed *in situ* at 250 and 400 °C, respectively. The base pressure of the EB evaporation chamber was below 1×10^{-7} Pa. Evaporation for each layer was performed at a substrate temperature of 150 °C.

Nano-structural analysis of the sputtered samples was performed by cross-sectional scanning transmission electron microscopy (STEM) with observation of nano-beam-electron diffraction (NBED) patterns and energy dispersive x-ray spectroscopy (EDS) (*Thermo Fisher Scientific* Titan G2 80-200 TEM). Magnetic properties were characterized using a vibrating sample magnetometer (VSM) and a superconducting quantum interference device VSM (SQUID-VSM). To elucidate the interface chemical states, the x-ray absorption spectroscopy (XAS) and x-ray magnetic circular dichroism (XMCD) measurements were performed by the total-electron-yield (TEY) mode at BL-7A in High-energy accelerator research organization (KEK), Photon Factory, using circularly polarized soft x-rays. The XAS spectra were obtained by changing the magnetic field with fixed beam helicity, which are defined as μ_+ and μ_-. The magnetic fields of ±1.0 T were applied parallel to the incident x-rays. The XAS and XMCD measurements were performed in the oblique incident setup at room temperature.

III. RESULTS

Figure 1 shows the cross-sectional annular dark-field (ADF)-STEM images of the sputtered samples for (a) the as-deposited sample and (b) the annealed sample at T_a = 500 °C. The material labels on the right side of the images were confirmed by the following EDS results. The ADF-STEM images show the epitaxial growth with the (001) orientation of the bcc Cr buffer (lower sides) and the fcc-like oxide layer (around the middle positions) for both the samples. Note that the Ru cap layers are polycrystalline with an hcp structure. Some misfit dislocations ("T" marks) were confirmed near the bcc/fcc interface, that is, Cr/Fe–Cr–O in the labels, within the observed region of the as-deposited sample in Fig. 1(a). The formation of the misfit dislocations is due to the in-plane lattice mismatch for bulk between (Cr, Fe) and MgO, that is, MgO has a ~4% larger lattice spacing. After annealing at T_a = 500 °C, the interface becomes much sharper and the lattice distortions within the oxide layer are suppressed, as shown in Fig. 1(b). The lattice matching at the interface of the annealed sample is also better than that of the as-deposited sample.

Figure 2 shows the EDS analysis results for (a) the as-deposited sample and (b) the annealed sample (T_a = 500 °C). Elemental maps with ADF-STEM images for Cr, Fe, O, Mg, and Ru are shown on the left, and the corresponding compositional profiles are shown on the right. As shown in Fig. 2(a), the Fe distribution overlaps with the O distribution, indicating significant diffusion and oxidation of Fe atoms during the film deposition. Unlike EB or molecular-beam epitaxy deposition, sputter deposition of MgO on Fe often promotes the surface oxidation of Fe; therefore, our sputtering condition of the MgO layer may have formed the Fe-oxide-based layer. The Cr interdiffusion may also originate from the MgO sputtering because of the high kinetic energies of the sputtered atoms. As a result, the fcc oxide

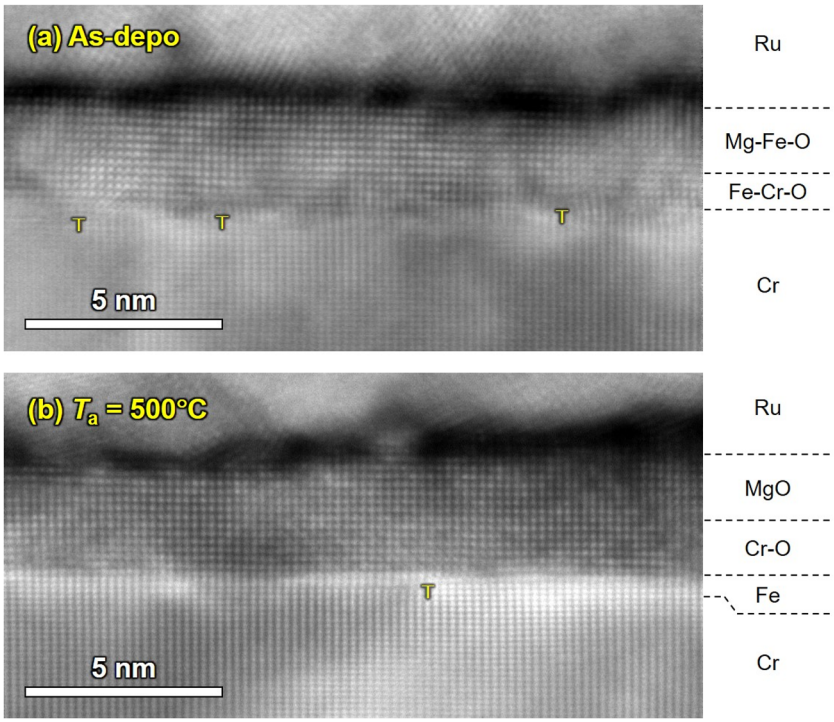

FIG. 1. Cross-sectional ADF-STEM images along MgO[100] direction of the sputtered samples with a Cr/Fe/MgO designed stack for (a) as-deposited and (b) T_a = 500 °C. "T" marks indicate misfit edge dislocations.

zone consisting of Fe–Cr–O and Mg–Fe–O with a gradual composition change was formed in the region between the Cr buffer and the Ru cap. After the annealing, as shown in Figs. 1(b) and 2(b), the Fe–Cr–O layer is partially reduced to form an ultrathin (~0.7 nm) Fe layer. With the formation of the Fe layer, the upper Mg–Fe–O layer also shows to the formation of MgO. It is also clearly confirmed that the Cr atoms remaining between the formed Fe and MgO layers segregate as a Cr oxide layer.

Figure 3 shows the NBED patterns of the as-deposited sample (upper) and the annealed sample (lower). Each pattern is taken

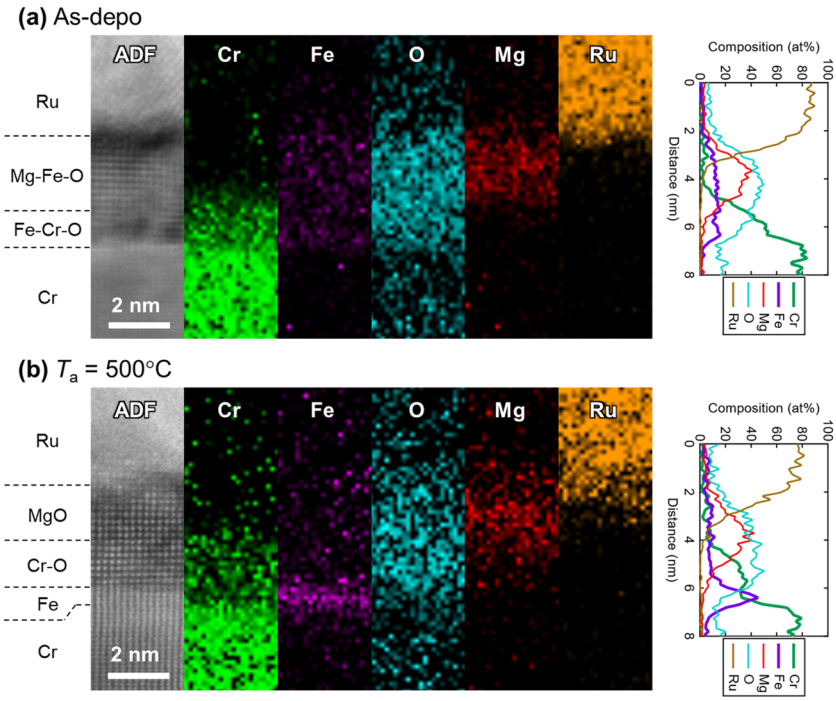

FIG. 2. EDS elemental maps with ADF-STEM images for Cr, Fe, O, Mg, and Ru (left images) and corresponding composition profiles (right plots) for (a) as-deposited and (b) T_a = 500 °C.

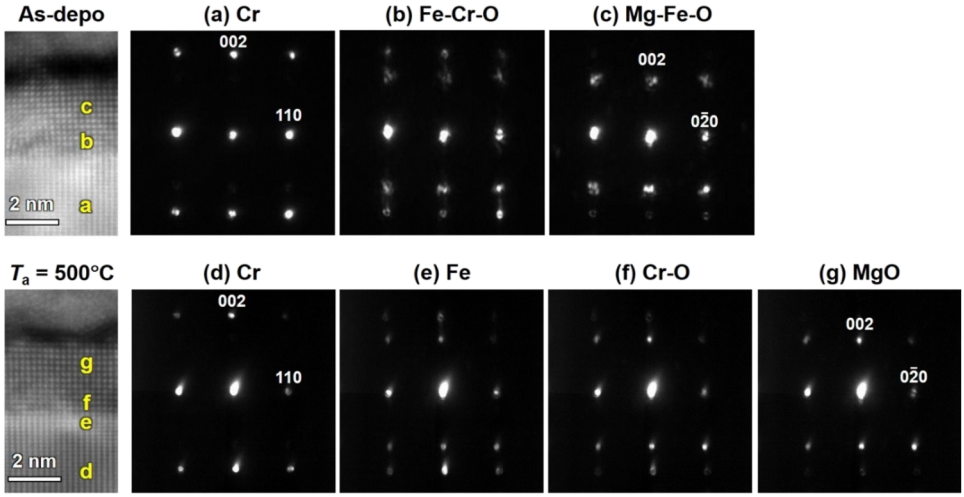

FIG. 3. NBED patterns of the sputtered samples taken from the respective positions of the ADF-STEM images on the left: (a) Cr, (b) Fe–Cr–O, and (c) Mg–Fe–O for the as-deposited sample; (d) Cr, (e) Fe, (f) Cr–O, and (g) MgO for the T_a = 500 °C annealed sample.

from the corresponding position of the HAADF-STEM images on the left side [labels (a)–(f)]. In both samples, the Cr buffers (a), (d) and the upper oxide layers (c), (g) have bcc(001) and fcc-based rock-salt(001) structures, respectively. The epitaxial relationship between the Cr and oxide layers is Cr(001)[110] and oxide(001)[100], as reported in previous studies.[4,16] As shown in Fig. 3(b), the overlapping patterns of bcc and fcc regions are observed in the Fe–Cr–O zone. The pattern of the Cr oxide layer of the annealed sample [Fig. 3(f)] is the same as that of the MgO layer, indicating that the layer has a rock-salt-type structure. Although Cr_2O_3 with an hcp-based corundum structure is the most stable among the Cr-based oxides, a metastable rock-salt CrO phase may be stabilized by the existence of the Fe(001) and MgO(001) interfaces in our samples. Note that the epitaxial relationship was determined to be Fe(001)[110]/CrO(001)[100]/MgO(001)[100]. A rock-salt $CrO_{0.87}$ phase with a lattice constant of 0.404 nm is reported in the literature,[29] which is nearly equal to the in-plane lattice spacing of Fe (0.404 nm, 45° in-plane rotation of bcc Fe) and smaller than that of MgO (0.421 nm). Therefore, the better lattice-matching in the annealed sample can be observed in Fig. 1(b).

Figures 4(a) and 4(b) show the magnetization (M)-magnetic field (H) curves for the samples with T_a = 300 and 500 °C, respectively. The red dashed line and blue solid line indicate the direction of the applied magnetic field along the in-plane and out-of-plane,

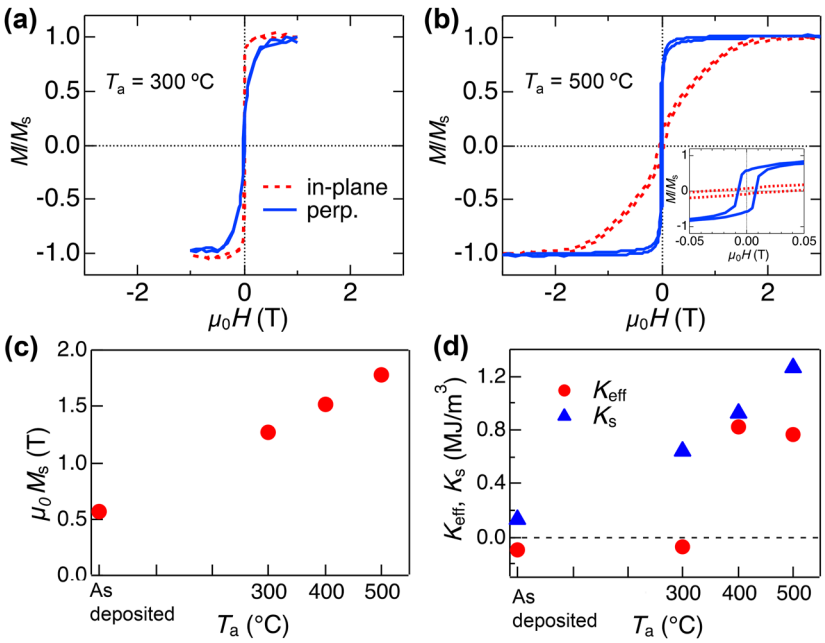

FIG. 4. M–H curves for the sputtered samples at (a) annealing temperature T_a = 300 °C and (b) 500 °C. T_a dependences of (c) M_s, and (d) K_{eff} and K_s. The inset of Fig. 4(b) shows the close-up near zero field.

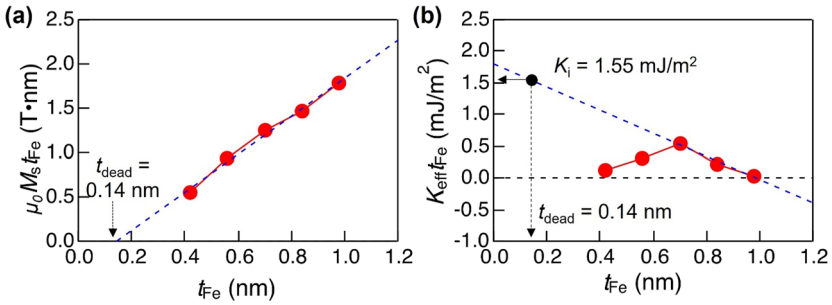

FIG. 5. t_{Fe} dependences of (a) products of M_s and t_{Fe} and (b) products of K_{eff} and t_{Fe} for T_a = 500 °C.

respectively. The effective magnetic anisotropy energy density (K_{eff}) was estimated by the area enclosed by the in-plane and out-of-plane M–H curves. When T_a is above 400 °C, large effective PMA energies K_{eff} were observed, where a positive K_{eff} indicates perpendicular magnetization. Since the Fe and MgO layers are separated by the CrO layer, the PMA appears at the Fe and CrO interface. The saturation magnetization (M_s) assuming the 0.7 nm Fe thickness clearly increases with T_a, as shown in Fig. 4(c). This result is reasonable considering the reduction of the fraction of the Fe oxide by post-annealing. K_{eff} for T_a = 400 and 500 °C is determined to be 0.82 and 0.77 MJ/m^3, respectively. Here, considering the shape magnetic anisotropy energy $K_s = M_s^2/2\mu_0$ (μ_0: permeability), these values are calculated to be 0.92 and 1.26 MJ/m^3 for the samples for T_a = 400 and 500 °C, respectively, as shown in Fig. 4(d). Note that the reference EB sample exhibits K_{eff} of 1.2 MJ/m^3, which is larger than the K_{eff} values of the sputtered samples. Since the K_s in thin films

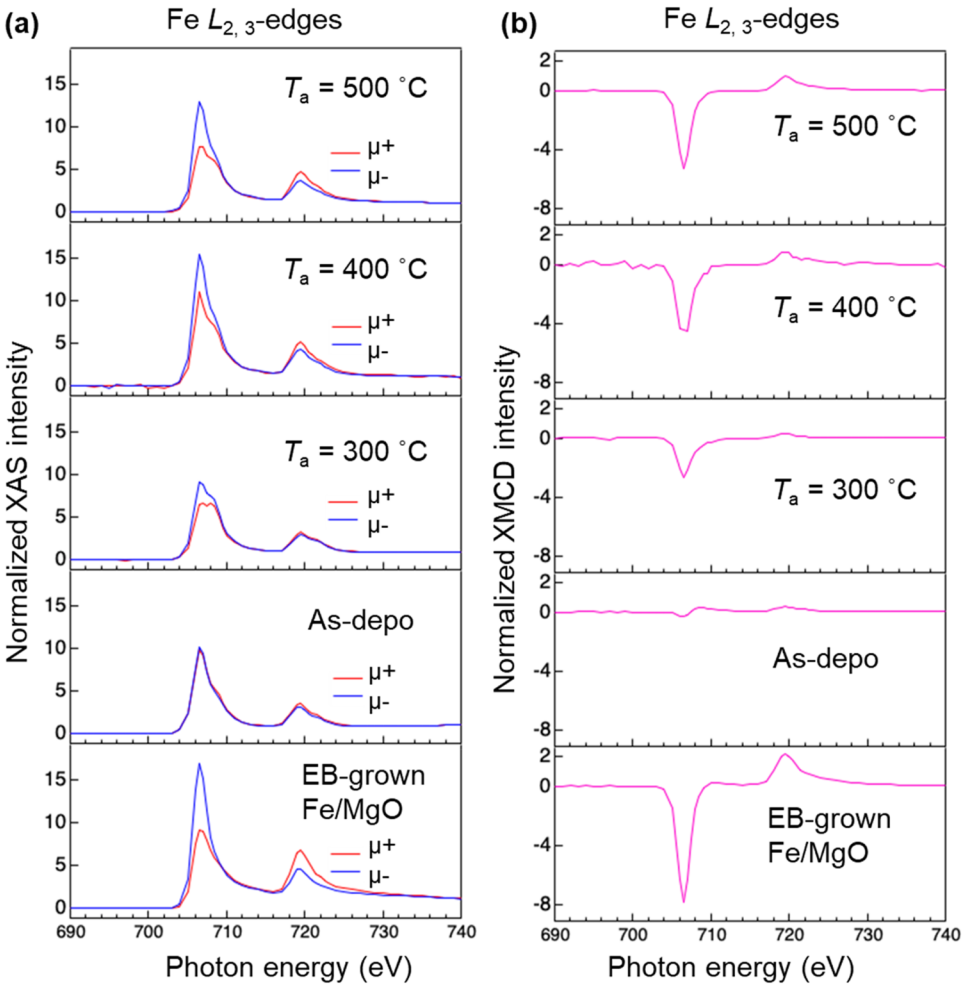

FIG. 6. (a) XAS and (b) XMCD of Fe $L_{2,3}$-edges taken at normal-incidence set up for the sputtered samples with different post-annealing temperatures and the reference EB sample.

stabilizes along the in-plane direction, the interfacial PMA energy (K_i) for T_a = 500 °C is larger than that for T_a = 400 °C. Therefore, we investigate the Fe thickness t_{Fe} dependences of magnetic properties. Figure 5 shows the t_{Fe} dependence of the products of M_s and t_{Fe} ($M_s \cdot t_{Fe}$) and the products of K_{eff} and t_{Fe} ($K_{eff} \cdot t_{Fe}$) of the sputtered samples for T_a = 500 °C. As shown in Fig. 5(a), the magnetic dead layer thickness (t_{dead}) of 0.14 nm was confirmed from the linear fit. The relationship between K_i and K_{eff} is expressed as $K_i = (K_{eff} - K_v) \cdot (t_{Fe} - t_{dead})$, where K_v is the volume magnetic anisotropy. K_i is estimated to be 1.55 mJ/m^2 from the linear fit shown in Fig. 5(b) (black dot). These results indicate that the unexpectedly formed Fe/CrO interface has relatively large PMA energies.

Figure 6 shows (a) XAS and (b) XMCD for Fe $L_{2,3}$-edges taken at normal-incidence set up in the sputtered samples with different T_a and the EB sample. The XAS and XMCD are defined as $(\mu_+ + \mu_-)/2$ and the difference of XAS, $\mu_+ - \mu_-$, respectively. In the Fe $L_{2,3}$-edges, the peaks at 706 and 719 eV originate from metallic Fe, and the peaks shifted to the higher energy side (707.5 and 721.5 eV) are due to the components of oxidized states. The XMCD peaks of the sputtered samples appear only at the metallic Fe energies and increase with T_a, which is consistent with the increase of M_s in VSM. The oxidized components are reduced after high temperature annealing. Note that the oxidized peaks cannot be detected in the EB sample as shown in the bottom panel of Fig. 6(a). Therefore, the chemical bonding nature is different between the sputtered sample with T_a = 500 °C and the EB sample. Figures 7(a) and 7(c) show the XAS taken at oblique-incidence set up for Fe and Cr $L_{2,3}$ edges, respectively, where the solid lines represent the sputtered samples with different T_a and the dotted lines represent the EB-grown sample. Figures 7(b) and 7(d) show the difference between the spectra of the sputtered samples and the spectra of the EB sample for Fe and Cr $L_{2,3}$ edges, respectively. These plots clearly show the degree of oxidation at the interface. The peak intensity of metallic Fe increases with annealing temperature, indicating that the chemical states of Fe oxide are significantly reduced by annealing. On the other hand, the spectra of the samples for T_a = 400 and 500 °C, which exhibit PMA, still show the presence of Fe oxide, as confirmed by Fig. 7(b). It is known that the over-oxidation of Fe at the oxide interface drastically reduces the PMA energy.[22,30] Therefore, the appearance of the large

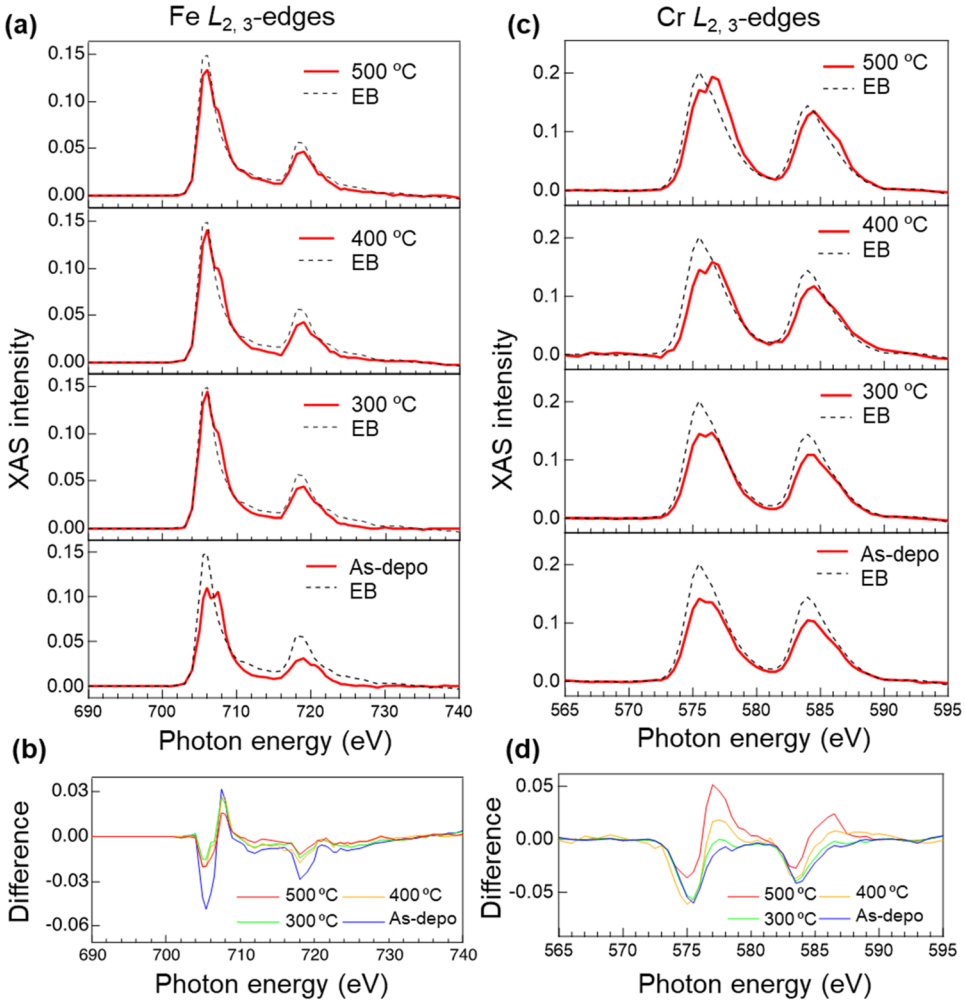

FIG. 7. XAS of (a) Fe and (b) Cr $L_{2,3}$-edges taken at oblique-incidence set up for the sputtered samples with different T_a and the reference EB sample. Dotted line represents XAS intensity of EB-grown sample. (b), (d) Differences of XAS intensity between sputtered samples and EB-grown sample.

PMA after the high temperature annealing indicates that the oxygen atoms may be uniformly located on the upper interface of the metallic Fe layer. In the XAS of Cr $L_{2,3}$-edges as shown in Fig. 7(c), the peaks at 575.5 and 584.5 eV indicate the metallic Cr and the peaks at 576.75 and 586.5 eV indicate the oxidized Cr states. It can be seen that the peak intensity due to the oxidation of Cr increases with T_a, as can be clearly seen in Fig. 7(d). In the Cr L_3-edge, the peak shift is 1.25 eV due to the oxidation of pure Cr, which is smaller than that of the Cr_2O_3 and CrO_2.[31–33] The peak shift of Cr^{2+} from metallic Cr is reported to be 1.8 eV.[34] Thus, the valence states of the Cr sites are deduced to be <2+, though the exact composition of CrO cannot be estimated from NBED and XAS. Although CrO is a metastable compound and the magnetic properties have not been investigated experimentally, the CrO was predicted to have an antiferromagnetic order from the band structure calculation.[35] XMCD of Cr was reported for Co/Cr_2O_3[36] and Fe/monolayer ordered Cr-oxide[37] by the induced moments at the interface. However, in our Fe/CrO, the Fe layer does not induce magnetic moments at Cr^{2+} sites.

IV. DISCUSSION

We discuss the mechanism of the CrO segregation at the Fe/MgO interface. From the viewpoint of the surface adsorption energy during growth and annealing, the possibility of Cr atom segregation on the Fe layer can be analyzed.[38,39] Here, the adsorption energy H_{ad}(A on B) is defined as the energy difference between the formation energy of the substrate surface B and the gas phase ad-atoms A. When H_{ad}(A on B) is larger than H_{ad} (B on B), the segregation of substrate atoms to the film surface can be realized.[38] As calculated in Ref. 38, since the energy difference between H_{ad}(Cr on Cr) (=303 kJ/mol) and H_{ad}(Cr on Fe) (=313 kJ/mol) is small, the segregation hardly occurs. In contrast, if the film is oxidized and the substrate has a higher affinity for oxygen, segregation can be promoted.[38] The Fe surface was oxidized during the MgO growth, and the Cr atoms have a higher affinity for oxygen than that for Fe.[39] Therefore, the oxygen atoms on the Fe surface act as a catalytic driving force, and the segregation of Cr atoms on the Fe surface occurs, resulting in the redox reaction of oxidized Fe to metallic Fe, which stabilizes the interface PMA, like the Fe/MgO interface. Similar phenomena of layer exchange growth can be observed in Si–Al, Si–Ag, and Ge–Al cases, which are annealed at temperatures below the eutectic point without forming an alloy.[40–42] Since Fe and Cr atoms do not form an alloy at 400–500 °C,[43] it is assumed that the Cr atoms diffuse to maintain the solid phase, and higher temperature annealing leads to alloy formation. Our experiment reveals that the interface obtained by a layer exchange process contributes to the PMA. Even for the combination of elements that are difficult to grow layer-by-layer in conventional sequential deposition methods, such a diffusion process can provide an alternative technique for preparing a well-controlled interface. For example, although it is difficult to grow an ultrathin Fe layer on MgO due to its poor wettability, the layer exchange process could provide an alternative. In addition, this method can produce metastable compounds such as CrO by diffusion into an interface.

Next, we discuss the PMA at the Fe/rock-salt-type CrO interface. Large interfacial PMA energies K_i of ~2 mJ/m^2 have been reported at Fe/MgO and $Fe/MgAl_2O_4$ interfaces.[4,24] The PMA energy of the $Fe/MgAl_2O_4$ interface is affected by the oxidation state; theoretical calculations show that both oxygen-poor and oxygen-rich interfaces result in reduced K_i compared to a perfect $Fe/MgAl_2O_4$ interface due to the reduced anisotropy of the orbital moment of Fe atoms.[44] It is also reported that the oxidation state significantly affects the PMA energies at CoFeB/Ta-oxide and CoFeB/(FeO, CoO) interfaces.[45,46] Theoretical calculations of Fe/MgO with monolayer FeO predicted that the PMA energy at the interface changes with the composition of FeO;[20] Fe/FeO/MgO shows in-plane magnetic anisotropy, while $Fe/FeO_{0.5}/MgO$ shows PMA.[20] Therefore, in an analogy to these facts, we expect that PMA appears at a well-defined Fe/CrO interface (depending on the oxygen composition) and can be explained by the formation of Fe–O chemical bonding exclusively in the normal direction to the interface through the orbital anisotropy.[47]

The interfacial PMA can be tuned by applying an external electric field, known as the voltage control magnetic anisotropy (VCMA) effect.[16,20,48–50] The degree of the VCMA effect (VCMA coefficient) of the Fe/MgO, also using EB evaporation, led to an improved PMA energy and VCMA coefficient.[51] The sample without Cr doping even showed a slight Cr segregation from the Cr buffer to the Fe/MgO interface region after the post-annealing. Although the state of segregated or doped Cr at the Fe/MgO interface is not clear, enhancement of both PMA and VCMA from pure Fe/MgO was reported at the Fe/Cr-doping/MgO interfaces. As predicted in $Fe/FeO_{0.5}/MgO$,[20] the enhancement could also be expected at the Fe/CrO interface depending on the oxygen composition.

The 3*d* transition-metal monoxides, including $CrO_{1-\delta}$ and $FeO_{1-\delta}$, are non-stoichiometric compounds with rock-salt-type structures, which have different magnetic ordering and conductivity,[41] and their lattice constants depend on the composition.[52–55] Since these lattice constants are almost the same as the in-plane lattice spacings of Fe, they can be incorporated into Fe-based MTJs. This suggests that it may be possible to realize interfacial PMA between Fe and transition-metal monoxide layers, which is a promising way to develop p-MTJs with additional functionality.[46]

V. CONCLUSION

We demonstrated interfacial PMA at the epitaxial Fe/rock-salt type Cr-oxide (CrO) (001) interface, which was formed by sputtering of a Cr/ultrathin Fe/MgO stacked sample. The Fe/CrO interface was formed via the atomic diffusion and redox reaction process of oxidized Fe and Cr with the aid of post-annealing, as revealed by STEM analysis and XAS measurements. A relatively large interfacial PMA energy of up to 1.55 mJ/m^2 was observed in the sample with annealing at T_a = 500 °C. This result indicates that the diffusion/redox process can provide high quality and well-controlled interfacial structures consisting of Fe-based FM and transition-metal-oxide. Our demonstration of the oxygen-driven diffusion process offers a new route to synthesize metastable materials in solid-state chemistry as well as an alternative technique for MTJ development.

ACKNOWLEDGMENTS

The authors thank Takayuki Nozaki for providing some useful comments based on Ref. 51. The authors thank Tomoya Nakatani

for fruitful discussion in the structural analysis. This work was partly supported by the JSPS KAKENHI (Grant Nos. 16H06332, 22H04966, 23K26535, and 24H00408). This paper is partly based on the results obtained from a Project commissioned by the New Energy and Industrial Technology Development Organization (NEDO) via Grant No. JPNP16007. Parts of the synchrotron radiation experiments were performed under the approval of the Photon Factory Program Advisory Committee, KEK (Grant No. 2021G069). Y.I. acknowledges the National Institute for Materials Science for the provision of the NIMS Graduate Research Assistantship.

AUTHOR DECLARATIONS

Conflict of Interest

The authors have no conflicts to disclose.

Author Contributions

Yuki Iida: Data curation (equal); Writing – original draft (equal). **Qingyi Xiang**: Data curation (supporting). **Thomas Scheike**: Data curation (supporting); Writing – review & editing (supporting). **Zhenchao Wen**: Data curation (supporting); Writing – review & editing (supporting). **Jun Okabayashi**: Conceptualization (equal); Data curation (equal); Investigation (equal); Writing – original draft (equal); Writing – review & editing (equal). **Jun Uzuhashi**: Data curation (equal); Formal analysis (equal). **Tadakatsu Ohkubo**: Data curation (supporting); Formal analysis (supporting). **Kazuhiro Hono**: Formal analysis (supporting). **Hiroaki Sukegawa**: Conceptualization (equal); Data curation (equal); Formal analysis (equal); Writing – original draft (equal); Writing – review & editing (equal). **Seiji Mitani**: Conceptualization (lead); Data curation (supporting); Formal analysis (supporting); Funding acquisition (lead); Writing – original draft (lead); Writing – review & editing (lead).

DATA AVAILABILITY

The data that support the findings of this study are available on request from the corresponding authors.

REFERENCES

[1]S. Yakata, H. Kubota, Y. Suzuki, K. Yakushiji, A. Fukushima, S. Yuasa, and K. Ando, "Influence of perpendicular magnetic anisotropy on spin-transfer switching current in CoFeB/MgO/CoFeB magnetic tunnel junctions," J. Appl. Phys. **105**, 07D131 (2009).

[2]S. Ikeda, K. Miura, H. Yamamoto, K. Mizunuma, H. D. Gan, M. Endo, S. Kanai, J. Hayakawa, F. Matsukura, and H. Ohno, "A perpendicular-anisotropy CoFeB–MgO magnetic tunnel junction," Nat. Mater. **9**, 721–724 (2010).

[3]D. C. Worledge, G. Hu, D. W. Abraham, J. Z. Sun, P. L. Trouilloud, J. Nowak, S. Brown, M. C. Gaidis, E. J. O'Sullivan, and R. P. Robertazzi, "Spin torque switching of perpendicular Ta-CoFeB-MgO-based magnetic tunnel junctions," Appl. Phys. Lett. **98**, 022501 (2011).

[4]J. W. Koo, S. Mitani, T. T. Sasaki, H. Sukegawa, Z. C. Wen, T. Ohkubo, T. Niizeki, K. Inomata, and K. Hono, "Large perpendicular magnetic anisotropy at Fe/MgO interface," Appl. Phys. Lett. **103**, 192401 (2013).

[5]J. Okabayashi, J. W. Koo, H. Sukegawa, S. Mitani, Y. Takagi, and T. Yokoyama, "Perpendicular magnetic anisotropy at the interface between ultrathin Fe film and MgO studied by angular-dependent x-ray magnetic circular dichroism," Appl. Phys. Lett. **105**, 122408 (2014).

[6]S. S. P. Parkin, C. Kaiser, A. Panchula, P. M. Rice, B. Hughes, M. Samant, and S.-H. Yang, "Giant tunnelling magnetoresistance at room temperature with MgO (100) tunnel barriers," Nat. Mater. **3**, 862 (2004).

[7]S. Yuasa, T. Nagahama, A. Fukushima, Y. Suzuki, and K. Ando, "Giant room-temperature magnetoresistance in single-crystal Fe/MgO/Fe magnetic tunnel junctions," Nat. Mater. **3**, 868 (2004).

[8]S. Ikeda, J. Hayakawa, Y. Ashizawa, Y. M. Lee, K. Miura, H. Hasegawa, M. Tsunoda, F. Matsukura, and H. Ohno, "Tunnel magnetoresistance of 604% at 300K by suppression of Ta diffusion in CoFeB/MgO/CoFeB pseudo-spin-valves annealed at high temperature," Appl. Phys. Lett. **93**, 082508 (2008).

[9]T. Scheike, Z. Wen, H. Sukegawa, and S. Mitani, "631% room temperature tunnel magnetoresistance with large oscillation effect in CoFe/MgO/CoFe(001) junctions," Appl. Phys. Lett. **122**, 112404 (2023).

[10]H. Kubota, A. Fukushima, Y. Ootani, S. Yuasa, K. Ando, H. Maehara, K. Tsunekawa, D. D. Djayaprawira, N. Watanabe, and Y. Suzuki, "Evaluation of spin-transfer switching in CoFeB/MgO/CoFeB magnetic tunnel junctions," Jpn. J. Appl. Phys. **44**, L1237 (2005).

[11]M. Yamanouchi, R. Koizumi, S. Ikeda, H. Sato, K. Mizunuma, K. Miura, H. D. Gan, F. Matsukura, and H. Ohno, "Dependence of magnetic anisotropy on MgO thickness and buffer layer in $Co_{20}Fe_{60}B_{20}$-MgO structure," J. Appl. Phys. **109**, 07C712 (2011).

[12]W. X. Wang, Y. Yang, H. Naganuma, Y. Ando, R. C. Yu, and X. F. Han, "The perpendicular anisotropy of $Co_{40}Fe_{40}B_{20}$ sandwiched between Ta and MgO layers and its application in CoFeB/MgO/CoFeB tunnel junction," Appl. Phys. Lett. **99**, 012502 (2011).

[13]Y.-W. Oh, K.-D. Lee, J.-R. Jeong, and B.-G. Park, "Interfacial perpendicular magnetic anisotropy in CoFeB/MgO structure with various underlayers," J. Appl. Phys. **115**, 17C724 (2014).

[14]W. Skowroński, T. Nozaki, D. D. Lam, Y. Shiota, K. Yakushiji, H. Kubota, A. Fukushima, S. Yuasa, and Y. Suzuki, "Underlayer material influence on electric-field controlled perpendicular magnetic anisotropy in CoFeB/MgO magnetic tunnel junctions," Phys. Rev. B **91**, 184410 (2015).

[15]P. J. Chen, Y. L. Iunin, S. F. Cheng, and R. D. Shull, "Underlayer effect on perpendicular magnetic anisotropy in $Co_{20}Fe_{60}B_{20}$/MgO films," IEEE Trans. Magn. **52**, 4400504 (2016).

[16]T. Nozaki, A. Kozioł-Rachwał, W. Skowroński, V. Zayets, Y. Shiota, S. Tamaru, H. Kubota, A. Fukushima, S. Yuasa, and Y. Suzuki, "Large voltage-induced changes in the perpendicular magnetic anisotropy of an MgO-based tunnel junction with an ultrathin Fe layer," Phys. Rev. Appl. **5**, 044006 (2016).

[17]J. Sinha, M. Hayashi, A. J. Kellock, S. Fukami, M. Yamanouchi, H. Sato, S. Ikeda, S. Mitani, S. Yang, S. S. P. Parkin, and H. Ohno, "Enhanced interface perpendicular magnetic anisotropy in Ta|CoFeB|MgO using nitrogen doped Ta underlayers," Appl. Phys. Lett. **102**, 242405 (2013).

[18]K.-M. Lee, J. W. Choi, J. Sok, and B.-C. Min, "Temperature dependence of the interfacial magnetic anisotropy in W/CoFeB/MgO," AIP Adv. **7**, 065107 (2017).

[19]P. Bruno, "Tight-binding approach to the orbital magnetic moment and magnetocrystalline anisotropy of transition-metal monolayers," Phys. Rev. B **39**, 865 (1989).

[20]K. Nakamura, T. Akiyama, T. Ito, M. Weinert, and A. J. Freeman, "Role of an interfacial FeO layer in the electric-field-driven switching of magnetocrystalline anisotropy at the Fe/MgO interface," Phys. Rev. B **81**, 220409 (2010).

[21]M. K. Niranjan, C.-G. Duan, S. S. Jaswal, and E. Y. Tsymbal, "Electric field effect on magnetization at the Fe/MgO(001) interface," Appl. Phys. Lett. **96**, 222504 (2010).

[22]H. X. Yang, M. Chshiev, B. Dieny, J. H. Lee, A. Manchon, and K. H. Shin, "First-principles investigation of the very large perpendicular magnetic anisotropy at Fe|MgO and Co|MgO interfaces," Phys. Rev. B **84**, 054401 (2011).

[23]Y. Miura, M. Tsujikawa, and M. Shirai, "A first-principles study on magnetocrystalline anisotropy at interfaces of Fe with non-magnetic metals," J. Appl. Phys. **113**, 233908 (2013).

[24]Q. Xiang, R. Mandal, H. Sukegawa, Y. K. Takahashi, and S. Mitani, "Large perpendicular magnetic anisotropy in epitaxial Fe/$MgAl_2O_4$(001) heterostructures," Appl. Phys. Express **11**, 063008 (2018).

[25]K. Masuda and Y. Miura, "Perpendicular magnetic anisotropy at the Fe/$MgAl_2O_4$ interface: Comparative first-principles study with Fe/MgO," Phys. Rev. B **98**, 224421 (2018).

[26]H. Sukegawa, J. P. Hadorn, Z. Wen, T. Ohkubo, S. Mitani, and K. Hono, "Perpendicular magnetic anisotropy at lattice-matched $Co_2FeAl/MgAl_2O_4(001)$ epitaxial interfaces," Appl. Phys. Lett. **110**, 112403 (2017).
[27]J. P. Hadorn, H. Sukegawa, T. Ohkubo, S. Mitani, and K. Hono, "Microstructural evolution of perpendicular magnetization films with an ultrathin $Co_2FeAl/MgAl_2O_4(001)$ structure," Acta Mater. **145**, 306 (2018).
[28]S. Kobayashi, H. Koizumi, H. Yanagihara, J. Okabayashi, T. Kondo, T. Kubota, K. Takanashi, and Y. Sonobe, "Perpendicular magnetic anisotropy of an ultrathin Fe layer grown on NiO(001)," Phys. Rev. Appl. **19**, 064005 (2023).
[29]D. Alontseva, E. Ghassemieh, A. Russakova, A. Krassavin, and N. Prokhorenkova, "Developing a new resource and energy saving technology of precision application of powder coating multifunctional systems," Acta Phys. Pol., A **134**, 374 (2018).
[30]Y. Iida, J. Okabayashi, and S. Mitani, "Perpendicular magnetic anisotropy in sputter-deposited Fe/MgO interfaces tuned by W buffer and Tb capping layers," Appl. Phys. Lett. **113**, 252401 (2018).
[31]M. C. Biesinger, C. Brown, J. R. Mycroft, R. D. Davidson, and N. S. McIntyre, "X-ray photoelectron spectroscopy studies of chromium compounds," Surf. Interface Anal. **36**, 1550 (2004).
[32]S. Seong, E. Lee, H. W. Kim, B. I. Min, S. Lee, J. Dho, Y. Kim, J.-Y. Kim, and J.-S. Kang, "Experimental evidence for mixed-valent Cr ions in half-metallic CrO_2: Temperature-dependent XMCD study," J. Magn. Magn. Mater. **452**, 447 (2018).
[33]M. Asa, G. Vinai, J. L. Hart, C. Autieri, C. Rinaldi, P. Torelli, G. Panaccione, M. L. Taheri, S. Picozzi, and M. Cantoni, "Interdiffusion-driven synthesis of tetragonal chromium (III) oxide on $BaTiO_3$," Phys. Rev. Mater. **2**, 033401 (2018).
[34]C. Xu, M. Hassel, H. Kuhlenbeck, and H.-J. Freund, "Adsorption and reaction on oxide surfaces: NO, NO_2 on $Cr_2O_3(111)/Cr(110)$," Surf. Sci. **258**, 23 (1991).
[35]J. Liu, T. Yang, A. Xu, R. L. Martin, Y. Yang, H. Jiao, Y. Li, and X.-D. Wen, "Predication of screened hybrid functional on transition metal monoxides: From Mott insulator to charge transfer insulator," J. Alloys Compd. **808**, 151707 (2019).
[36]K. Toyoki, Y. Shiratsuchi, T. Nakamura, C. Mitsumata, S. Harimoto, Y. Takechi, T. Nishimura, H. Nomura, and R. Nakatani, "Equilibrium surface magnetization of α-Cr_2O_3 studied through interfacial chromium magnetization in Co/α-Cr_2O_3 layered structures," Appl. Phys. Express **7**, 114201 (2014).
[37]A. Brambilla, G. Berti, A. Calloni, A. Picone, M. Riva, G. Bussetti, S. Nappini, E. Magnano, M. Finazzi, L. Duò, and F. Ciccacci, "Magnetic properties of monolayer range chromium oxides on Fe(001)," J. Appl. Phys. **114**, 123905 (2013).
[38]M. Yoshitake, Y.-R. Aparna, and K. Yoshihara, "General rule for predicting surface segregation of substrate metal on film surface," J. Vac. Sci. Technol., A **19**, 1432 (2001).
[39]M. Yoshitake, "Prediction of influence of oxygen in annealing atmosphere on surface segregation behavior in layered materials," Jpn. J. Appl. Phys. **51**, 085601 (2012).
[40]O. Nast, T. Puzzer, L. M. Koschier, A. B. Sproul, and S. R. Wenham, "Aluminum-induced crystallization of amorphous silicon on glass substrates above and below the eutectic temperature," Appl. Phys. Lett. **73**, 3214 (1998).
[41]M. Scholz, M. Gjukic, and M. Stutzmann, "Silver-induced layer exchange for the low-temperature preparation of intrinsic polycrystalline silicon films," Appl. Phys. Lett. **94**, 012108 (2009).
[42]K. Toko, M. Kurosawa, N. Saitoh, N. Yoshizawa, N. Usami, M. Miyao, and T. Suemasu, "Highly (111)-oriented Ge thin films on insulators formed by Al-induced crystallization," Appl. Phys. Lett. **101**, 072106 (2012).
[43]S.-L. Chen, J.-Y. Zhang, X.-G. Lu, K.-C. Chou, and Y. A. Chang, "Application of Graham scan algorithm in binary phase diagram calculation," J. Phase Equilib. Diffus. **27**, 121 (2006).
[44]R. Mandal, Q. Xiang, K. Masuda, Y. Miura, H. Sukegawa, S. Mitani, and Y. K. Takahashi, "Spin-resolved contribution to perpendicular magnetic anisotropy and Gilbert damping in interface-engineered $Fe/MgAl_2O_4$ heterostructures," Phys. Rev. Appl. **14**, 064027 (2020).
[45]G. Yu, L.-T. Chang, M. Akyol, P. Upadhyaya, C. He, X. Li, K. L. Wong, P. K. Amiri, and K. L. Wang, "Current-driven perpendicular magnetization switching in Ta/CoFeB/[TaO_x or MgO/TaO_x] films with lateral structural asymmetry," Appl. Phys. Lett. **105**, 102411 (2014).
[46]M. Xu, M. Li, P. Khanal, A. Habiboglu, B. Insana, Y. Xiong, T. Peterson, J. C. Myers, D. Ortega, H. Qu, C. L. Chien, W. Zhang, J.-P. Wang, and W. G. Wang, "Voltage-controlled antiferromagnetism in magnetic tunnel junctions," Phys. Rev. Lett. **124**, 187701 (2020).
[47]Y. Miura and J. Okabayashi, "Understanding magnetocrystalline anisotropy based on orbital and quadrupole moments," J. Phys.: Condens.Matter **34**, 473001 (2022).
[48]T. Maruyama, Y. Shiota, T. Nozaki, K. Ohta, N. Toda, M. Mizuguchi, A. A. Tulapurkar, T. Shinjo, M. Shiraishi, S. Mizukami, Y. Ando, and Y. Suzuki, "Large voltage-induced magnetic anisotropy change in a few atomic layers of iron," Nat. Nanotechnol. **4**, 158 (2009).
[49]Y. Shiota, T. Nozaki, F. Bonell, S. Murakami, T. Shinjo, and Y. Suzuki, "Induction of coherent magnetization switching in a few atomic layers of FeCo using voltage pulses," Nat. Mater. **11**, 39 (2012).
[50]Q. Xiang, Z. Wen, H. Sukegawa, S. Kasai, T. Seki, T. Kubota, K. Takanashi, and S. Mitani, "Nonlinear electric field effect on perpendicular magnetic anisotropy in Fe/MgO interfaces," J. Phys. D: Appl. Phys. **50**, 40LT04 (2017).
[51]A. Kozioł-Rachwał, T. Nozaki, K. Freindl, J. Korecki, S. Yuasa, and Y. Suzuki, "Enhancement of perpendicular magnetic anisotropy and its electric field-induced change through interface engineering in Cr/Fe/MgO," Sci. Rep. **7**, 5993 (2017).
[52]M. Akimitsu, T. Mizoguchi, J. Akimitsu, and S. Kimura, "Magnetic structure and magnetic properties of non-stoichiometric $Fe_{1-x}O$," J. Phys. Chem. Solids **44**, 497 (1983).
[53]M. Saeki and M. Nakahira, "Superstructure of VO_x in the range, x = 1.15–1.25, and its stability," Mater. Res. Bull. **6**, 603 (1971).
[54]F. F. Ferreira, M. H. Tabacniks, M. C. A. Fantini, I. C. Faria, and A. Gorenstein, "Electrochromic nickel oxide thin films deposited under different sputtering conditions," Solid State Ionics **86–88**, 971 (1996).
[55]O. Banakh, P. E. Schmid, R. Sanjinés, and F. Lévy, "Electrical and optical properties of TiO_x thin films deposited by reactive magnetron sputtering," Surf. Coat. Technol. **151–152**, 272 (2002).